PERGAMON

International Journal of Solids and Structures 40 (2003) 6593–6612

INTERNATIONAL JOURNAL OF SOLIDS and STRUCTURES

www.elsevier.com/locate/ijsolstr

Multiple reciprocity boundary element analysis of two-dimensional anisotropic thermoelasticity involving an internal arbitrary non-uniform volume heat source

Y.C. Shiah *, Y.J. Lin

Department of Aeronautical Engineering, Feng Chia University, 100 Wenhwa Road, Seatwen 407, Taichung, Taiwan, ROC

Received 13 April 2003; received in revised form 5 August 2003

Abstract

In the direct boundary element method (BEM) formulation of anisotropic thermoelasticity, thermal loads manifest themselves as additional volume integral terms in the boundary integral equation (BIE). Conventionally, this requires internal cell discretisation throughout the whole domain. In this paper, the multiple reciprocity method in BEM analysis is employed to treat the general 2D thermoelasticity problem when the thermal loading is due to an internal non-uniform volume heat source. By successively performing the "volume-to-surface" integral transformation, the general formulation of the associated BIE for the problem is derived. The successful implementation of such a scheme is illustrated by three numerical examples.

Keywords: Multiple reciprocity boundary element method; Anisotropic thermoelasticity; Non-uniform volume heat source

1. Introduction

Materials with anisotropic properties are increasingly being used in engineering applications and much attention has been paid to the stress analysis of such materials. In a number of thermoelasticity problems in engineering, internal volume heat sources with non-uniform heat generation rates may be present in the anisotropic media due to, for example, internal chemical reactions or electrical heating. Although some analytical solutions have been obtained for a few specific problems (see e.g., Sherief and Magahed, 1999; Dhaliwal and Sherief, 1980), recourse to numerical methods is generally necessary for most problems in practice.

Among the general numerical methods for engineering analysis, the boundary element method (BEM) has been recognized as an efficient computational tool. This is due to its distinctive feature of requiring only the numerical discretisation of the boundary of the solution domain. In the direct BEM formulation for

* Corresponding author. Tel.: +886-4-2451/7250x3956; fax: +886-4-2451-0862.
E-mail address: ycshiah@fcu.edu.tw (Y.C. Shiah).

0020-7683/$ - see front matter © 2003 Elsevier Ltd. All rights reserved.
doi:10.1016/j.ijsolstr.2003.08.006

elastostatics, however, body-force and thermal elastic effects are well known to manifest themselves as additional volume integral terms. The direct means of treating these integrals will require internal cell discretisation throughout the whole domain. Such a direct evaluation by volume discretisation would, however, destroy the notion of BEM as the boundary solution technique. Several schemes have been proposed over the years to resolve this "volume integral problem" in the BEM analysis of isotropic, elastic bodies when inertia and thermal effects are considered. The simplest way of computing the domain integral is by subdividing the region into a series of internal cells, on each of which the Gauss quadrature scheme is applied. Alternatively, Gipson and Camp (1985) and Camp and Gipson (1992) employed an integration scheme based on the Monte Carlo method whereby a system of random integration points rather than a regular integration grid is used. Another way to avoid computing the domain integral is to apply particular solutions (see, e.g., Lachat, 1975; Deb and Banerjee, 1990) by changing the variables in such a manner that the domain integral disappears from the boundary integral equation (BIE). The dual reciprocity method, proposed by Nardini and Brebbia (1982), has also been widely applied to deal with volume integrals. Perhaps the most analytically elegant approach is the exact transformation method (ETM) (see, e.g., Rizzo and Shippy, 1977; Tan, 1983; and Danson, 1983), sometimes referred to as the Galerkin vector approach, in which the "volume integral" is transformed exactly into a series of boundary ones. Generalizing the Galerkin vector approach with a set of higher-order fundamental solutions, the multiple reciprocity method (MRM) was introduced by Nowak (1989) for the transient heat conduction problem and later extended to a series of other applications by Nowak and Brebbia (1989). Among the schemes mentioned above, the ETM and MRM are fundamentally most appealing because they restore the BEM analysis as a purely boundary solution technique yet without requiring further numerical approximations.

Although the ETM has been widely employed to treat the volume integrals associated with body-force and thermal effects in isotropic elasticity, similar transformations for anisotropic elasticity have not been successfully achieved until very recently. The works of Zhang et al. (1996a,b, 1997) were the first reported successful attempts to consider the inertia effect. The effect of a temperature change in the elastic body can, in essence, be treated as an effective body-force over the solution domain in Navier's equations of equilibrium. Notwithstanding this, the extension of the ETM to handle these effects in an anisotropic medium is not as straightforward as in isotropic elasticity. This is because, unlike the potential function for body-force, the distribution of a temperature change in an anisotropic body, in the general case, does not satisfy the standard Poisson's equation. The difficulties arising from this were not overcome until very recently when Shiah and Tan (1999a) transformed the "volume integral", in the analytically exact sense, into a series of boundary ones. By removing the singularity at the source point for interior stress calculations, Shiah and Tan (1999b) also derived the Somigliana's identity of the interior strain for 2D anisotropic thermoelasticity. Although the particular integral approach has been employed by Deb et al. (1991) to treat 2D anisotropic thermoelasticity, the technique involves sub-dividing a domain into "volume cells". In each of these cells, the temperature field is approximated by a suitable polynomial function through a multiple regression analysis. In order to obtain satisfactory results, the particular integrals need to be judiciously chosen.

In this article, the MRM is applied to treat 2D anisotropic thermoelasticity under steady state conditions when the volume heat source is within the domain. The recurrence formulae employing a set of higher-order anisotropic fundamental solutions are derived to treat the volume integral arising from the thermal loading of an internal arbitrary volume heat source in the anisotropic medium. The heat generation rate of the volume heat source can be of any form of a continuous function. However, the formulations presented would not be applicable to domains with the presence of discrete point heat sources. This is mainly due to the singularity of temperature field near the heat sources that invalidates the analytical transformation for the volume integral. To consider discrete point heat sources is outside the scope of the present study and still remains at work in progress. In general, for a random distribution of heat generation rate, a continuous function to represent the distribution needs to be chosen through the multiple regression analysis. This is not within the scope of the present study. By applying the principal of MRM, the process to successively

convert the volume integral associated with the thermal loading follows the same vein as the procedures described in the work by Shiah and Tan (1999a). This scheme has been successfully implemented into BEM codes based on the quadratic isoparametric element formulation used in 2D anisotropic thermoelasticity. A brief review of the procedure to treat the associated 2D anisotropic field problem in BEM is presented next. This is followed by the formulation of the exact transformation process using the MRM. The successful implementation of the proposed scheme is then illustrated by three numerical examples.

2. 2D anisotropic heat conduction

As a pre-process to deal with the problem of coupled anisotropic thermoelasticity, the corresponding anisotropic heat conduction problem must first be solved to determine the distribution of the temperature and its spatial gradients. With an internal volume heat source, the governing partial differential equation for the 2D anisotropic heat conduction problem may be expressed as

$$K_{ij}\Theta_{,ij}+H(x,y)=0 \tag{1}$$

where Θ represents a temperature change, the function $H(x,y)$ denotes the known function for the distribution of internal heat generation rate; K_{ij} are the thermal conductivity coefficients which, from thermodynamic principals and Onsagar's reciprocity relation, have the following relationships,

$$K_{11}>0,\quad K_{22}>0,\quad K_{11}K_{22}-K_{12}^2>0,\quad K_{12}=K_{21} \tag{2}$$

In the case of orthotropy, where the cross-derivative term in Eq. (1) is absent, the analysis can be considerably simplified. As a result, the conventional way to numerically treat the fully anisotropic problem has been to determine the principal axes by rotation of the original Cartesian coordinates so that this term disappears. By employing the method of characteristics to transform the governing equation into the standard Laplace's form, Shiah and Tan (1997) successfully solved the anisotropic heat conduction problem using the isotropic boundary integral equation. The linear transformation between both coordinate systems may be generally expressed as

$$[\hat{x}_1 \quad \hat{x}_2]^{\mathrm{T}}=[F(K_{ij})][x_1 \quad x_2]^{\mathrm{T}},\quad [x_1 \quad x_2]^{\mathrm{T}}=[F^{-1}(K_{ij})][\hat{x}_1 \quad \hat{x}_2]^{\mathrm{T}} \tag{3}$$

where $[F(K_{ij})]$ (or $[F^{-1}(K_{ij})]$), the transformation (or the inverse transformation) matrix in terms of the invariant coefficients, has its component element $[F_{mn}(K_{ij})]$ (or $[F_{mn}^{-1}(K_{ij})]$). The linear transformation allows the analysis to be carried out using any standard BEM codes for the isotropic potential theory, albeit on a distorted domain in the mapped plane. As is presented in detail by Shiah and Tan (1997), the mapping takes the following form,

$$\mathbf{F}=\begin{pmatrix}\sqrt{\Delta}/K_{11} & 0\\ -K_{12}/K_{11} & 1\end{pmatrix},\quad \mathbf{F^{-1}}=\begin{pmatrix}K_{11}/\sqrt{\Delta} & 0\\ K_{12}/\sqrt{\Delta} & 1\end{pmatrix},\quad \Delta=K_{11}K_{22}-K_{12}^2 \tag{4}$$

Through the transformation described above, the anisotropic field involving an internal volume heat source is now governed by

$$\Theta_{,\underline{ii}}=-H\left(F_{11}^{-1}\hat{x}_1+F_{12}^{-1}\hat{x}_2,F_{21}^{-1}\hat{x}_1+F_{22}^{-1}\hat{x}_2\right)K_{11}/\Delta=\widehat{H}_1(\hat{x}_1,\hat{x}_2) \tag{5}$$

which is the standard Poisson's equation in the mapped plane. The associated anisotropic field problem may now be solved by MRM (Nowak and Brebbia, 1989) in conjunction with the direct domain mapping technique (Shiah and Tan, 1997).

3. 2D anisotropic thermoelastic BIE

For a brief review of the basic boundary integral equation for 2D anisotropic thermoelasticity, consider the direct formulation of the BEM for an anisotropic solid in two-dimensions, where the displacements, u_i, and the tractions, t_i, on the boundary S of the domain Ω, are related by

$$C_{ij}u_i(P) + \int_S u_i(Q)T_{ij}(P,Q)\,\mathrm{d}S = \int_S t_i(Q)U_{ij}(P,Q)\,\mathrm{d}S + \int_\Omega X_i(q)U_{ij}(P,q)\,\mathrm{d}\Omega \tag{6}$$

in which Q and q represent the field points on S and in Ω, respectively, and P represents the source point on S. In Eq. (6), C_{ij} are the coefficients associated with boundary geometry at the source point P. Also in Eq. (6), X_i represents the equivalent body-force term due to the temperature change in the domain, and $U_{ij}(P,q)$ is the displacement fundamental solution, given by

$$U_{ij}(P,q) = 2\mathrm{Re}\{r_{i1}A_{j1}\log z_1 + r_{i2}A_{j2}\log z_2\} \tag{7}$$

Also, $T_{ij}(P,Q)$ is the corresponding traction fundamental solution, which is well established in BEM literature (see e.g., Tan et al., 1992). In Eq. (7), r_{ij} and A_{ji} are material constants, expressed by complex quantities, $\mathrm{Re}\{\cdot\}$ is the operator which takes the real part of these quantities, and z_i is a generalized complex variable defined in terms of the characteristic roots, μ_i, and the difference of coordinates between the field point $Q(x_1,x_2)$ and the load or source point $P(x_{p1},x_{p2})$ as follows

$$z_i = (x_1 - x_{p1}) + \mu_i(x_2 - x_{p2}) = \zeta_1 + \mu_i\zeta_2 \tag{8}$$

In Eq. (8), ζ_i represent the local coordinates which have the origin located at the source point. If the temperature change of the elastic body is Θ, the equivalent body-force X_i can then be written as $X_i = -\gamma_{ij}\Theta_{,j}$ where γ_{ij} are the coefficients given by $\gamma_{ij} = c_{ijkl}\alpha_{kl}$, c_{ijkl} being the material stiffness matrix and α_{kl} being the coefficients of thermal expansion. Substituting this and the additional thermal traction term into Eq. (6), the complete integral equation considering thermal effects can now be expressed as

$$C_{ij}u_i(P) + \int_S u_i(Q)T_{ij}(P,Q)\,\mathrm{d}S = \int_S t_i(Q)U_{ij}(P,Q)\,\mathrm{d}S + \int_S \gamma_{ik}n_k\Theta U_{ij}(P,Q)\,\mathrm{d}S - \int_\Omega \gamma_{ik}\Theta_{,k}U_{ij}(P,q)\,\mathrm{d}\Omega \tag{9}$$

As can be seen, the last term on the right-hand-side of Eq. (9) is a volume integral arising from the thermal loading. To restore the notion of the BEM as a computational boundary solution technique, the volume integral (VI) needs to be transformed into boundary ones.

4. Exact VI transformation by MRM

With the heat conduction equation now defined in the $\hat{x}_i$-coordinate system and in the form of Eq. (5), the volume integral transformation of the term due to the thermal loading in Eq. (9) can be performed following the same procedures by Shiah and Tan (1999a). Only the main steps will be described here as the details have been presented in this reference. Recall that the VI term is

$$\mathrm{VI}_j = -\int_\Omega \gamma_{ik}\Theta_{,k}U_{ij}\,\mathrm{d}\Omega \tag{10}$$

By expressing $\Theta_{,k}$ in the $\hat{x}_i$-coordinate system using the chain rule, Eq. (10) may be rewritten as

$$\mathrm{VI}_j = -\int_{\hat{\Omega}} \gamma_{\underline{ik}}\Theta_{,\underline{k}}U_{\underline{ij}}\,\mathrm{d}\hat{\Omega} \tag{11}$$

where the invariant coefficients $\gamma_{\underline{ij}}$ take the element of the matrix

$$\gamma_{\underline{ik}} = \begin{pmatrix} \gamma_{11} & \dfrac{-\gamma_{11}K_{12} + \gamma_{12}K_{11}}{\sqrt{\Delta}} \\ \gamma_{21} & \dfrac{-\gamma_{21}K_{12} + \gamma_{22}K_{11}}{\sqrt{\Delta}} \end{pmatrix} \tag{12}$$

Applying Green's first theorem to this integral results in

$$\mathrm{VI}_j = -\int_{\hat{\Omega}} \left[(\gamma_{\underline{ik}} U_{\underline{ij}} \Theta)_{,\underline{k}} - (\gamma_{\underline{ik}} U_{\underline{ij},\underline{k}} \Theta) \right] \mathrm{d}\widehat{\Omega} = -\int_{\hat{S}} (\gamma_{\underline{ik}} U_{ij} \Theta) n_{\underline{k}} \, \mathrm{d}\widehat{S} + \int_{\hat{\Omega}} (\gamma_{\underline{ik}} U_{\underline{ij},\underline{k}} \Theta) \, \mathrm{d}\widehat{\Omega} \tag{13}$$

It is convenient now to introduce a new function $Q_{\underline{ijk}}$ such that

$$Q_{\underline{ijk},\underline{tt}} = U_{\underline{ij},\underline{k}} \tag{14}$$

Recall Green's second identity,

$$\int_{\hat{\Omega}} (\phi \nabla^2 \varphi - \varphi \nabla^2 \phi) \, \mathrm{d}\widehat{\Omega} = \int_{\hat{S}} (\phi \nabla \varphi - \varphi \nabla \phi) \cdot \hat{\boldsymbol{n}} \, \mathrm{d}\widehat{S} \tag{15}$$

where $\hat{\boldsymbol{n}}$ denotes the unit outward normal at the boundary $\widehat{S}$. By substituting Θ for ϕ and $(\gamma_{\underline{ik}} Q_{\underline{ijk}})$ for φ, this identity can be rewritten as

$$\int_{\hat{\Omega}} (\gamma_{\underline{ik}} Q_{\underline{ijk},\underline{tt}} \Theta - \gamma_{\underline{ik}} Q_{\underline{ijk}} \Theta_{,\underline{tt}}) \, \mathrm{d}\widehat{\Omega} = \int_{\hat{S}} (\gamma_{\underline{ik}} Q_{\underline{ijk},\underline{t}} \Theta - \gamma_{\underline{ik}} Q_{\underline{ijk}} \Theta_{,\underline{t}}) n_{\underline{t}} \, \mathrm{d}\widehat{S} \tag{16}$$

Substituting Eq. (5) into Eq. (16) results in

$$\int_{\hat{\Omega}} (\gamma_{\underline{ik}} Q_{\underline{ijk},\underline{tt}} \Theta) \, \mathrm{d}\widehat{\Omega} = \int_{\hat{S}} (\gamma_{\underline{ik}} Q_{\underline{ijk},\underline{t}} \Theta - \gamma_{\underline{ik}} Q_{\underline{ijk}} \Theta_{,\underline{t}}) n_{\underline{t}} \, \mathrm{d}\widehat{S} + \int_{\hat{\Omega}} (V_{\underline{j}}^{(0)} \widehat{H}_1) \, \mathrm{d}\widehat{\Omega} \tag{17}$$

where $V_{\underline{j}}^{(0)}$ is used, for brevity, to represent the term $\gamma_{\underline{ik}} Q_{\underline{ijk}}$, and $\widehat{H}_1$ is the heat source function satisfying the associated heat conduction equation. To facilitate the volume integral transformation, a new function $V_{\underline{j}}^{(1)}$ is introduced such that it satisfies

$$\nabla^2 V_{\underline{j}}^{(1)} = V_{\underline{j}}^{(0)} \tag{18}$$

Substituting $V_{\underline{j}}^{(1)}$ for φ, and $\widehat{H}_1$ for ϕ, Green's identity, Eq. (15), can be rewritten as

$$\int_{\hat{\Omega}} \widehat{H}_1 \nabla^2 V_{\underline{j}}^{(1)} \, \mathrm{d}\widehat{\Omega} = \int_{\hat{S}} \left(\widehat{H}_1 V_{\underline{j},\underline{t}}^{(1)} - V_{\underline{j}}^{(1)} \widehat{H}_{1,\underline{t}} \right) \hat{n}_t \, \mathrm{d}\widehat{S} + \int_{\Omega} V_{\underline{j}}^{(1)} \widehat{H}_2 \, \mathrm{d}\widehat{\Omega} \tag{19}$$

where $\widehat{H}_2$ stands for

$$\widehat{H}_2 = \widehat{H}_{1,\underline{tt}} \tag{20}$$

In a similar manner, the transformation process may be successively performed to yield an infinite series as follows,

$$\int_{\hat{\Omega}} \widehat{H}_1 V_j^{(0)} \, \mathrm{d}\widehat{\Omega} = \sum_{m=1}^{\infty} \int_{\hat{S}} \left(\widehat{H}_m V_{\underline{j},\underline{t}}^{(m)} - V_{\underline{j}}^{(m)} \widehat{H}_{m,\underline{t}} \right) \hat{n}_t \, \mathrm{d}\widehat{S} \tag{21}$$

where $\widehat{H}_m$ is to denote the function taking $(m-1)$ times of Laplace's operation upon the heat source function $\widehat{H}_1$ in the mapped plane; $V_{\underline{j}}^{(m)}$ is defined to satisfy the following recursive relation,

$$\nabla^2 V_{\underline{j}}^{(m)} = V_{\underline{j}}^{(m-1)} \tag{22}$$

Therefore, from Eqs. (17) and (21), one may rewrite Eq. (13) in a form of boundary integrals as follows,

$$\mathrm{VI}_j = -\int_{\hat{S}} (\gamma_{\underline{ik}} U_{ij} \Theta) n_{\underline{k}} \,\mathrm{d}\widehat{S} + \int_{\hat{S}} (\gamma_{\underline{ik}} Q_{\underline{ijk},\underline{t}} \Theta - \gamma_{\underline{ik}} Q_{\underline{ijk}} \Theta_{,\underline{t}}) n_{\underline{t}} \,\mathrm{d}\widehat{S} + \sum_{m=1}^{\infty} \int_{\hat{S}} \left(\widehat{H}_m V_{\underline{j},\underline{t}}^{(m)} - V_{\underline{j}}^{(m)} \widehat{H}_{m,\underline{t}} \right) \hat{n}_t \,\mathrm{d}\widehat{S} \tag{23}$$

For evaluating the boundary integrals in the infinite series, the task remains to determine the general explicit form of $V_{\underline{j}}^{(m)}$ as well as $V_{\underline{j},\underline{t}}^{(m)}$ in a similar manner as was done by Shiah and Tan (1999a). For this purpose, it is worth examining how the generalized complex variable $z(\mu)$ may be expressed in terms of the parameters in the $\hat{x}_i$-coordinate system. The general form of Eq. (8) may be rewritten as

$$z_i = \mu_{ji}(x_j - x_{pj}) \tag{24}$$

where μ_{ji} represents elements of the matrix

$$\mu_{ji} = \begin{pmatrix} 1 & 1 \\ \mu_1 & \mu_2 \end{pmatrix} \tag{25}$$

By expressing the generalized complex variable in the $\hat{x}_i$-coordinate system, Eq. (24) may be rewritten as

$$z_{\underline{i}} = \mu_{\underline{ji}}(\hat{x}_j - \hat{x}_{pj}) \tag{26}$$

where, using Eqs. (3) and (4), it can be easily shown that $\mu_{\underline{ji}}$ is given by

$$\mu_{\underline{ji}} = \begin{pmatrix} \dfrac{K_{11} + \mu_1 K_{12}}{\sqrt{\Delta}} & \dfrac{K_{11} + \mu_2 K_{12}}{\sqrt{\Delta}} \\ \mu_1 & \mu_2 \end{pmatrix} \tag{27}$$

Differentiating $U_{\underline{ij}}$ with respect to the field point Q in the $\hat{x}_i$-coordinate system yields

$$U_{\underline{ij},\underline{k}} = 2\mathrm{Re}\{r_{i1} A_{j1} \mu_{\underline{k}1}/z_{\underline{1}} + r_{i2} A_{j2} \mu_{\underline{k}2}/z_{\underline{2}}\} \tag{28}$$

From Eqs. (14) and (28), the function $Q_{\underline{ijk}}$ is found to be

$$Q_{\underline{ijk}} = 2\mathrm{Re}\left\{ \frac{r_{i1} A_{j1} \mu_{\underline{k}1} z_{\underline{1}} \log(z_{\underline{1}})}{(\mu_{\underline{1}1}^2 + \mu_{\underline{2}1}^2)} + \frac{r_{i2} A_{j2} \mu_{\underline{k}2} z_{\underline{2}} \log(z_{\underline{2}})}{(\mu_{\underline{2}1}^2 + \mu_{\underline{2}2}^2)} \right\} \tag{29}$$

From direct differentiation, its spatial derivative that appears in Eq. (23) can be readily determined to be

$$Q_{\underline{ijk},\underline{t}} = 2\mathrm{Re}\left\{ \frac{r_{i1} A_{j1} \mu_{\underline{k}1} \mu_{\underline{t}1} z_{\underline{1}} \log(z_{\underline{1}})}{(\mu_{\underline{1}1}^2 + \mu_{\underline{2}1}^2)} + \frac{r_{i2} A_{j2} \mu_{\underline{k}2} \mu_{\underline{t}2} z_{\underline{2}} \log(z_{\underline{2}})}{(\mu_{\underline{2}1}^2 + \mu_{\underline{2}2}^2)} \right\} \tag{30}$$

From the definition $V_{\underline{j}}^{(0)} = \gamma_{\underline{ik}} Q_{\underline{ijk}}$, one may readily obtain

$$V_{\underline{j}}^{(0)} = 2\gamma_{\underline{ik}} \mathrm{Re}\left\{ \frac{r_{i1} A_{j1} \mu_{\underline{k}1} z_{\underline{1}} \log(z_{\underline{1}})}{(\mu_{\underline{1}1}^2 + \mu_{\underline{2}1}^2)} + \frac{r_{i2} A_{j2} \mu_{\underline{k}2} z_{\underline{2}} \log(z_{\underline{2}})}{(\mu_{\underline{2}1}^2 + \mu_{\underline{2}2}^2)} \right\} \tag{31}$$

Eq. (18) implies that the explicit form of $V_{\underline{j}}^{(1)}$ is expressed as

$$V_{\underline{j}}^{(1)} = 2\gamma_{\underline{ik}} \mathrm{Re}\left\{ \frac{r_{i1} A_{j1} \mu_{\underline{k}1}}{(\mu_{\underline{1}1}^2 + \mu_{\underline{2}1}^2)} \left[F_1 z_{\underline{1}}^3 \log(z_{\underline{1}}) + F_2 z_{\underline{1}}^3 \right] + \frac{r_{i2} A_{j2} \mu_{\underline{k}2}}{(\mu_{\underline{2}1}^2 + \mu_{\underline{2}2}^2)} \left[F_3 z_{\underline{2}}^3 \log(z_{\underline{2}}) + F_4 z_{\underline{2}}^3 \right] \right\} \tag{32}$$

where F_1–F_4 are invariant coefficients to be determined from Eq. (18). Following the same procedure as in Zhang et al. (1996a,b, 1997) to determine the coefficients, one may obtain

$$F_1 = \frac{1}{6(\mu_{\underline{1}1}^2 + \mu_{\underline{2}1}^2)}, \quad F_2 = \frac{-5}{36(\mu_{\underline{1}1}^2 + \mu_{\underline{2}1}^2)}, \quad F_3 = \frac{1}{6(\mu_{\underline{1}2}^2 + \mu_{\underline{2}2}^2)}, \quad F_4 = \frac{-5}{36(\mu_{\underline{1}2}^2 + \mu_{\underline{2}2}^2)} \tag{33}$$

By repeating the same procedure successively to determine the fundamental solution of a higher-order form for $V_{\underline{j}}$, one may obtain the general form of $V_{\underline{j}}$ in the nth order as

$$V_{\underline{j}}^{(n)} = 2\gamma_{\underline{ik}}\mathrm{Re}\left\{ \frac{r_{i1}A_{j1}\mu_{\underline{k1}}}{(\mu_{\underline{11}}^2+\mu_{\underline{21}}^2)^{n+1}}\left[G_1^{(n)}z_{\underline{1}}^{2n+1}\log(z_{\underline{1}})+G_2^{(n)}z_{\underline{1}}^{2n+1}\right] + \frac{r_{i2}A_{j2}\mu_{\underline{k2}}}{(\mu_{\underline{21}}^2+\mu_{\underline{22}}^2)^{n+1}}\left[G_1^{(n)}z_{\underline{2}}^{2n+1}\log(z_{\underline{2}})+G_2^{(n)}z_{\underline{2}}^{2n+1}\right]\right\}, \quad (n=0,1,\ldots,\infty) \tag{34}$$

where the coefficients $G_1^{(n)}$ and $G_2^{(n)}$ are given by the following recurrence formulae,

$$G_1^{(n+1)} = \frac{G_1^{(n)}}{4n^2+10n+6}, \quad G_2^{(n+1)} = \frac{G_2^{(n)}}{4n^2+10n+6} - \frac{G_1^{(n)}(4n+5)}{(4n^2+10n+6)^2} \quad G_1^{(0)}=1, \quad G_2^{(0)}=0, \quad (n=0,1,\ldots,\infty) \tag{35}$$

Differentiation of $V_{\underline{j}}^{(n)}$ yields

$$V_{\underline{j},\underline{t}}^{(n)} = 2\gamma_{\underline{ik}}\mathrm{Re}\left\{ \frac{r_{i1}A_{j1}\mu_{\underline{k1}}\mu_{\underline{t1}}}{(\mu_{\underline{11}}^2+\mu_{\underline{21}}^2)^{n+1}}\left[(2n+1)G_1^{(n)}z_{\underline{1}}^{2n+1}\log(z_{\underline{1}})+(G_1^{(n)}+2nG_2^{(n)}+G_2^{(n)})z_{\underline{1}}^{2n+1}\right] + \frac{r_{i2}A_{j2}\mu_{\underline{k2}}\mu_{\underline{t2}}}{(\mu_{\underline{21}}^2+\mu_{\underline{22}}^2)^{n+1}}\left[(2n+1)G_1^{(n)}z_{\underline{2}}^{2n+1}\log(z_{\underline{2}})+(G_1^{(n)}+2nG_2^{(n)}+G_2^{(n)})z_{\underline{2}}^{2n+1}\right]\right\} \tag{36}$$

which appears in Eq. (23). In the presence of an internal arbitrary volume heat source, the complete boundary integral equation for 2D anisotropic thermoelasticity can now be rewritten as

$$\begin{aligned} C_{ij}u_i(P)+\int_S u_i(Q)T_{ij}(P,Q)\,\mathrm{d}S &= \int_S t_i(Q)U_{ij}(P,Q)\,\mathrm{d}S+\int_S \gamma_{ik}n_kU_{ij}(P,Q)\Theta\,\mathrm{d}S-\int_{\hat{S}}\gamma_{\underline{ik}}n_{\underline{k}}U_{ij}(P,Q)\Theta\,\mathrm{d}\widehat{S} \\ &\quad+\int_{\hat{S}}\left[\gamma_{\underline{ik}}Q_{\underline{ijk},\underline{t}}(P,Q)\Theta-\gamma_{\underline{ik}}Q_{\underline{ijk}}(P,Q)\Theta_{,\underline{t}}\right]n_{\underline{t}}\,\mathrm{d}\widehat{S}+\sum_{m=1}^{\infty}\int_{\hat{S}}\left(\widehat{H}_mV_{\underline{j},\underline{t}}^{(m)}(P,Q)\right. \\ &\quad\left.-V_{\underline{j}}^{(m)}(P,Q)\widehat{H}_{m,\underline{t}}\right)\hat{n}_t\,\mathrm{d}\widehat{S} \end{aligned} \tag{37}$$

In Eq. (37), by incorporating the integral terms containing $Q_{\underline{ijk},\underline{t}}$ and $Q_{\underline{ijk}}$ into the infinite series, the above equation can be further abbreviated into a simpler form,

$$\begin{aligned} C_{ij}u_i(P)+\int_S u_i(Q)T_{ij}(P,Q)\,\mathrm{d}S &= \int_S t_i(Q)U_{ij}(P,Q)\,\mathrm{d}S+\int_S \gamma_{ik}n_kU_{ij}(P,Q)\Theta\,\mathrm{d}S-\int_{\hat{S}}\gamma_{\underline{ik}}n_{\underline{k}}U_{ij}(P,Q)\Theta\,\mathrm{d}\widehat{S} \\ &\quad+\sum_{n=0}^{\infty}\int_{\hat{S}}\left(\widehat{H}_nV_{\underline{j},\underline{t}}^{(n)}(P,Q)-V_{\underline{j}}^{(n)}(P,Q)\widehat{H}_{n,\underline{t}}\right)\hat{n}_t\,\mathrm{d}\widehat{S} \end{aligned} \tag{38}$$

in which $\widehat{H}_0$ (when $n=0$) is defined by $\widehat{H}_0=\Theta$. To determine $\widehat{H}_j$ directly from its definition, one needs to successively perform Laplace's operation upon the heat source function $\widehat{H}_1$, which should be explicitly known for a specific distribution. Inspecting the recurrence formulae in Eq. (35), one may observe that the factor $(4n^2+10n+6)$ appears in the denominators of the coefficients and hence guarantees rapid convergence of the infinite series. In general, the infinite series have been tested to converge to a finite value for most heat source functions when n is set no more than 7. When the heat source function reveals strong divergence for $\widehat{H}_n$, properly re-scaling of the domain dimensions may be necessary to ensure rapid convergence of the infinite series. For this re-scaling process, all nodal coordinates may be divided by the

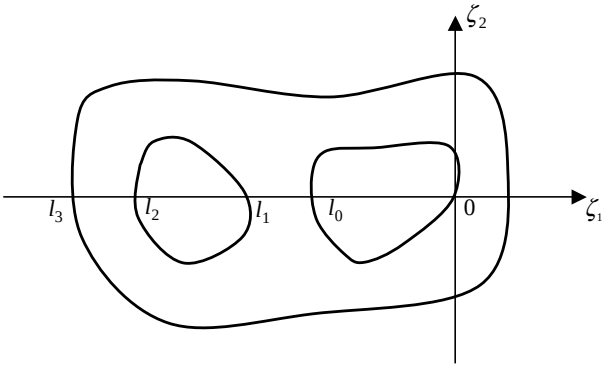

Fig. 1. A multiply connected domain.

maximum length between any two arbitrary nodes such that $\widehat{H}_n$ is convergent for taking $n-1$ times of Laplace's operations upon the heat source function. With all functions determined, solving Eq. (38) presents no serious difficulties since all integrands are at most weakly singular.

There remains one more issue that needs to be addressed in the general case, however. It concerns the terms containing $\log(z)$ in the integrands, as it may not be analytic everywhere in the domain. This issue has been explained in detail in Zhang et al. (1996b), and Shiah and Tan (1999a); thus, it will only be briefly discussed here. If one defines the principal value of z as $-\pi < \arg(z) \leqslant \pi$, the quantity $\log(z)$ is not analytic along the negative ζ_1-axis. This will invalidate the foregoing VI transformation. Although the problem may be avoided by argument redefinition as proposed by Zhang et al. (1996b), it is not always possible to redefine the range of $\arg(z)$ to ensure the analyticity of $\log(z)$ everywhere in the domain. This is true for a multiply connected domain. Take the region shown in Fig. 1, for example. If rays from any point along an inner boundary are projected in arbitrary directions, they will cut through the domain. By carrying out a limiting process in their work on body-force loading, Zhang et al. (1996b) resolved this problem and obtained a series of extra line integrals over the intervals along the negative ζ_1-axis where it cuts the domain, such as (l_0, l_1), (l_2, l_3), from the source point on the internal surface of the region. These extra line integrals along the negative ζ_1-axis serve to restore the analyticity of the surface integrals by cancelling out the terms arising from the discontinuity of $\log(z)$ along that axis. The same limiting process may be followed to obtain the extra line integrals for thermal loading. Also, this can be done by summing up the surface integrals along the negative ζ_1-axis for the upper and the lower domain with proper arguments, i.e., $+\pi$ for the upper domain and $-\pi$ for the lower domain. In the general case, if the negative ζ_1-axis cuts through the region m times in the intervals $(l_{2m-1}, l_{2m-2}), (l_{2m-3}, l_{2m-3}), \ldots, (l_1, l_0)$, the complete boundary integral equation for plane anisotropic thermoelasticity with an internal arbitrary volume heat source can be shown to be as follows,

$$\begin{aligned} C_{ij}u_i(P) + \int_S u_i(Q)T_{ij}(P,Q)\,\mathrm{d}S = {} & \int_S t_i(Q)U_{ij}(P,Q)\,\mathrm{d}S + \int_S \gamma_{ik}n_k U_{ij}(P,Q)\Theta\,\mathrm{d}S - \int_{\widehat{S}} \gamma_{\underline{ik}}n_{\underline{k}}U_{ij}(P,Q)\Theta\,\mathrm{d}\widehat{S} \\ & + \sum_{n=0}^{\infty}\int_{\widehat{S}} \left(\widehat{H}_n V^{(n)}_{\underline{j},\underline{t}}(P,Q) - V^{(n)}_{\underline{j}}(P,Q)\widehat{H}_{n,\underline{t}}\right)\hat{n}_t\,\mathrm{d}\widehat{S} \\ & + \sum_{n=0}^{\infty}\sum_{k=1}^{m}\int_{l_{2k-1}}^{l_{2k-2}} L^{(n)}_j(\zeta_1)\,\mathrm{d}\zeta_1 \end{aligned} \tag{39}$$

where the integrand, $L_j^{(n)}(\zeta_1)$, for the extra line integrals is

$$L_j^{(n)}(\zeta_1) = -4\pi\Theta\left(\frac{k_{12}}{k_{11}}\gamma_{i\underline{1}} + \frac{\sqrt{\Delta}}{k_{11}}\gamma_{i\underline{2}}\right)\mathrm{Im}\{r_{i1}A_{j1} + r_{i2}A_{j2}\} + 4\pi(2n+1)\widehat{H}_n G_1^{(n)}\zeta_1^{2n}\gamma_{i\underline{k}}$$
$$\times\left(\frac{K_{12}}{K_{11}}\mathrm{Im}\left\{\frac{r_{i1}A_{j1}\mu_{\underline{1}1}\mu_{\underline{k}1}}{(\mu_{\underline{1}1}^2+\mu_{\underline{2}1}^2)^{n+1}} + \frac{r_{i2}A_{j2}\mu_{\underline{1}2}\mu_{\underline{k}2}}{(\mu_{\underline{1}2}^2+\mu_{\underline{2}2}^2)^{n+1}}\right\} + \frac{\sqrt{\Delta}}{k_{11}}\mathrm{Im}\left\{\frac{r_{i1}A_{j1}\mu_{\underline{2}1}\mu_{\underline{k}1}}{(\mu_{\underline{1}1}^2+\mu_{\underline{2}1}^2)^{n+1}} + \frac{r_{i2}A_{j2}\mu_{\underline{2}2}\mu_{\underline{k}2}}{(\mu_{\underline{1}2}^2+\mu_{\underline{2}2}^2)^{n+1}}\right\}\right)$$
$$-4\pi G_1^{(n)}\zeta_1^{2n+1}\gamma_{i\underline{k}}\left(\widehat{H}_{\underline{1}}\frac{k_{12}}{k_{11}} + \widehat{H}_{\underline{2}}\frac{\sqrt{\Delta}}{k_{11}}\right)\mathrm{Im}\left\{\frac{r_{i1}A_{j1}\mu_{\underline{k}1}}{(\mu_{\underline{1}1}^2+\mu_{\underline{2}1}^2)^{n+1}} + \frac{r_{i2}A_{j2}\mu_{\underline{k}2}}{(\mu_{\underline{1}2}^2+\mu_{\underline{2}2}^2)^{n+1}}\right\} \quad (40)$$

In Eq. (40), $\mathrm{Im}\{\cdot\}$ is the operator that takes the imaginary part of the complex quantities in the parentheses. In what follows, the veracity as well as the applicability of the derived formulations will be illustrated by three numerical examples.

5. Numerical examples

In this section, three test examples are investigated that involve thermal loading of an internal volume hear source presented in a fully anisotropic, elastic medium. The proposed approach to treat the volume integral arising from the thermal loading of an internal arbitrary volume heat source has been implemented into an existing BEM computer code based on the quadratic isoparametric element formulation. Simply for the purpose of verification of the derived formulae by means of direct evaluation of the domain integral, the first problem analyzed is assumed to have a trigonometric temperature distribution that corresponds to a specific volume heat source function. The associated volume integral is evaluated by the present ETM approach and also by the direct domain integration method (DIM) using the commercial software MATHCAD for a comparison of integration results. The second is a square plate with a central hole subjected to an unknown temperature distribution corresponding to a field problem under prescribed boundary conditions, while the third is a thin square plate, partially loaded with an internal square volume heat source. Albeit fictitious, the distribution functions of the heat generation rate for these examples are principally to demonstrate the mathematical soundness as well as the generality of the proposed scheme. For a random distribution of the heat generation rate in real engineering practice, it may involve the multiple regression analysis to determine an appropriate heat source function for each different problem. For the present analyses, eight terms ($n = 0$–7) of the infinite series are employed, which are quite enough for most continuous heat source functions.

The first example is designed basically for demonstration of the validity of the derived formulae, while the others are to show the generality as well as the applicability of the proposed scheme. Using the usual notations but with asterisks denoting values in the directions of the principal axes, the material properties for the first problem are arbitrarily chosen to have the following values,

E_{11}^*/E_{22}^*	v_{12}^*	G_{12}^*/E_{22}^*	$\eta_{12,1}^*$	$\eta_{12,2}^*$	$\alpha_{11}^*/\alpha_{22}^*$	K_{11}/K_{12}	K_{22}/K_{12}
36/18	0.32	8.2/18	0	0	2.3/4.0	4/5	25/5

In the other two examples, the material properties are chosen to correspond to a glass-epoxy to show the applicability of this technique for practical materials and they are

E_{11}^*/E_{22}^*	v_{12}^*	G_{12}^*/E_{22}^*	$\eta_{12,1}^*$	$\eta_{12,2}^*$	$\alpha_{11}^*/\alpha_{22}^*$	K_{11}^*/K_{22}^*
55/21	0.25	9.7/21	0	0	6.3/20.0	3.46/0.35

The second example is to consider a doubly connected region and the last one deals with a thin square plate partially loaded with an internal heat source. Both problems demand the extra line integrals to restore the validity of the volume-to-surface integral transformation, while the last one further involves the conventional sub-regioning technique. For verifications of the obtained results, the last two problems are also solved by ANSYS6.0, commercial software based on the finite element method.

5.1. Example 1

As shown in Fig. 2, consider a thin square plate with dimensions $W \times W$ ($W = 2$) that is subjected to a distribution of temperature change $\Theta = x_1^2 \sin x_2$. For the purpose of verifying the developed formulae, suppose the heat source function bears the form,

$$H(x_1, x_2) = (25x_1^2 - 8)\sin x_2 - 20x_1 \cos x_2 \tag{41}$$

which satisfies the governing heat conduction equation with the assumed conductivity coefficients. The material principal axes are arbitrarily taken to be oriented 30° counterclockwise with respect to the global Cartesian axes to account for full anisotropy as shown in Fig. 2. Also, Fig. 2 shows the boundary element mesh used where there are 16 quadratic isoparametric elements with a total of 32 nodes to model the boundary.

The volume integral associated with the thermal loading is evaluated by the boundary integrals in Eq. (39) and also by the direct domain integration performed using commercial software MATHCAD6.0 for comparison. The results, normalized by the largest distance between any two nodes in the mesh, $\sqrt{2}W$, are shown in Table 1 for comparison. As can be seen from the comparison of both results in the table, the excellent agreement between both results verifies the veracity of the series of boundary integrals and the recurrence formulae derived for the volume-to-surface integral transformation.

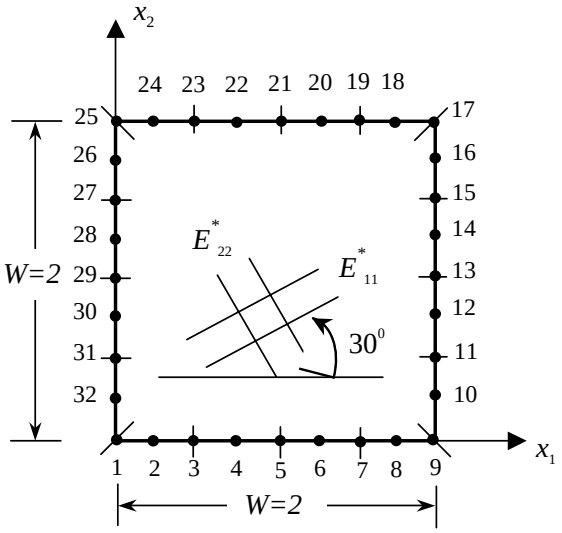

Fig. 2. Boundary element mesh for Problem 1.

Table 1
Numerical values of the normalized volume integral, $VI_j/\sqrt{2}W$—Problem 1

Node	$VI_1/W\sqrt{2}$		$VI_2/W\sqrt{2}$	
	ETM	DIM	ETM	DIM
1	0.15221E−05	0.15221E−05	−0.11600E−05	−0.11603E−05
2	0.14129E−05	0.14104E−05	−0.04196E−05	−0.04191E−05
3	0.13349E−05	0.13313E−05	−0.05639E−05	−0.05636E−05
4	0.12993E−05	0.12948E−05	−0.06972E−05	−0.06968E−05
5	0.13153E−05	0.13109E−05	−0.08026E−05	−0.08015E−05
6	0.13889E−05	0.13858E−05	−0.08552E−05	−0.08528E−05
7	0.15194E−05	0.15187E−05	−0.08213E−05	−0.08162E−05
8	0.16945E−05	0.16950E−05	−0.06553E−05	−0.06479E−05
9	0.18754E−05	0.18734E−05	−0.02995E−05	−0.02985E−05
10	0.13191E−05	0.13167E−05	−0.04778E−05	−0.04777E−05
11	0.07299E−05	0.07264E−05	−0.05603E−05	−0.05588E−05
12	0.02009E−05	0.01947E−05	−0.05650E−05	−0.05634E−05
13	−0.02031E−05	−0.02091E−05	−0.05128E−05	−0.05126E−05
14	−0.04220E−05	−0.04306E−05	−0.04323E−05	−0.04296E−05
15	−0.04206E−05	−0.04276E−05	−0.03425E−05	−0.03383E−05
16	−0.01631E−05	−0.01719E−05	−0.02654E−05	−0.02621E−05
17	0.02573E−05	0.02677E−05	−0.00491E−05	−0.00601E−05
18	0.02938E−05	0.03051E−05	0.01185E−05	0.01094E−05
19	0.03473E−05	0.03878E−05	0.14931E−05	0.14546E−05
20	0.04281E−05	0.04390E−05	0.02881E−05	0.02823E−05
21	0.06312E−05	0.06404E−05	0.04538E−05	0.04507E−05
22	0.08769E−05	0.08848E−05	0.06074E−05	0.06065E−05
23	0.11455E−05	0.11517E−05	0.07423E−05	0.07426E−05
24	0.14183E−05	0.14233E−05	0.08538E−05	0.08552E−05
25	0.16794E−05	0.16794E−05	0.09432E−05	0.09431E−05
26	0.13723E−05	0.13722E−05	0.07820E−05	0.07820E−05
27	0.11296E−05	0.11295E−05	0.05857E−05	0.05857E−05
28	0.09765E−05	0.09764E−05	0.03759E−05	0.03759E−05
29	0.09214E−05	0.09213E−05	0.01737E−05	0.01736E−05
30	0.09618E−05	0.09618E−05	−0.00029E−05	−0.00031E−05
31	0.10869E−05	0.10869E−05	−0.01407E−06	−0.01408E−05
32	0.12801E−05	0.12801E−05	−0.02316E−05	−0.02317E−05

5.2. Example 2

The preceding example has been chosen such that the mathematical soundness of the developed formulations can be readily verified using the direct domain integration performed by MATHCAD. As a more complicated example to demonstrate the involvement of the extra line integrals for a multiply connected region, the second problem, as schematically depicted in Fig. 3, is to consider a thin square plate with a central hole subjected to the thermal loading due to a volume heat generation rate described by

$$H(x_1, x_2)/K^*_{22} = 285.71429\cosh(0.41023x_1)\exp(x_2 - 0.50202x_1) \tag{42}$$

which is arbitrarily chosen to demonstrate the generality of the developed formulations in accounting for an arbitrary heat generation rate. Fig. 3 also shows the contours of such a distribution with darker regions illustrating higher heat generation rates. Unlike the first problem with an assumed temperature function, the plate reaches a steady-state temperature field with the thermal boundary conditions prescribed as follows. Two opposite sides, AB and CD, of the plate have a temperature change $\Theta = 100°$, while the inner

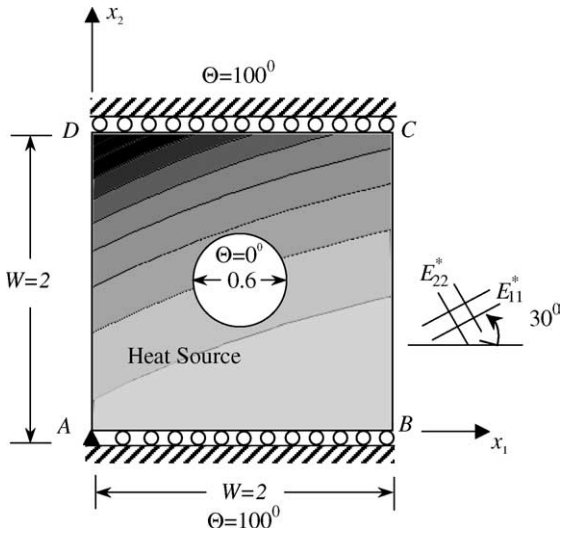

Fig. 3. A thin anisotropic plate with a hole subjected to a non-uniform volume heat generation rate.

surface of the hole is maintained at its original temperature ($\Theta = 0°$); the other two surfaces, AD and BC, are thermally insulted. All geometrical dimensions are shown in Fig. 3. With reference to this figure, sides AB and CD are restrained from displacement in the x_2-direction, while the other two surfaces BC and AD are free to move in any direction. To prevent rigid body motion, point A is also restrained in the x_1-direction. Also, as schematically depicted in Fig. 3, the principal axes of both material and thermal properties are arbitrarily chosen to be oriented 30° counterclockwise with respect to the global Cartesian axes to account for full anisotropy.

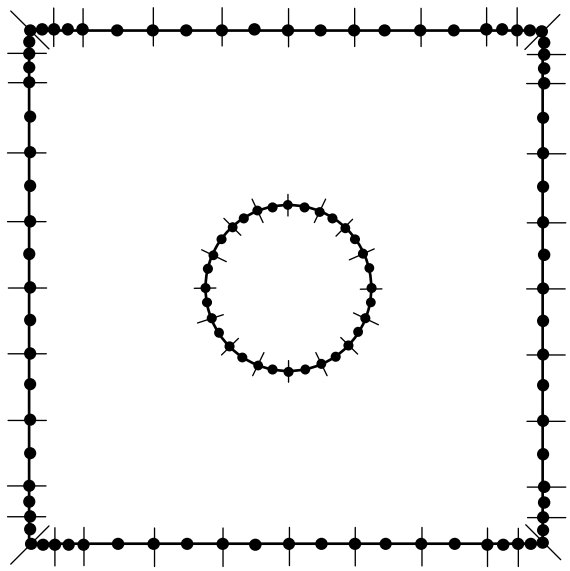

Fig. 4. BEM mesh of domain treated as a multiply connected region—Example 2.

As shown in Fig. 4, a total of 56 quadratic isoparametric elements with 112 nodes are applied to model the domain. As is usual for analyzing any statically coupled thermoelastic problem, the associated anisotropic temperature field problem is first solved for the distribution of temperature and its gradients at all boundary nodes. This is carried out using the MRM (Nowak and Brebbia, 1989) in conjunction with the direct domain mapping technique (Shiah and Tan, 1997). Instead of applying the conventional sub-regioning technique to resolve the analytical issue of the logarithmic function $\log z_i$ as aforementioned, the boundary integral equation with the extra line integrals, given by Eq. (39), is employed to demonstrate the veracity of the developed formulations. Any field values, such as the temperature and its gradients, at interior points required by the extra line integrals is computed in the BEM code for solving the associated anisotropic field problem. In ANSYS, the domain is discretized into 2048 PLANE77 elements, for each of which a constant heat source with the strength corresponding to the given heat generation function at its center is prescribed to simulate the continuous distribution of the heat generation rate. Fig. 5 shows the domain modeling by ANSYS. Computations of the normalized stresses, $\sigma_{11}/E^*_{11}\alpha^*_{11}\Theta_0$ and $\sigma_{22}/E^*_{11}\alpha^*_{11}\Theta_0$, along AB and CD are carried out by both schemes and the obtained results are shown in Figs. 6 and 7, respectively. The variations of the computed normalized stresses, $\sigma_{22}/E^*_{11}\alpha^*_{11}\Theta_0$, along BC and AD are plotted in Fig. 8. Also, the normalized hoop stresses are calculated along the circumference of the inside hole and plotted in Fig. 9 for both results obtained by BEM and FEM. It can be obviously seen that to our satisfactions, the BEM results obtained by the developed formulations indeed agree with those obtained by FEM very well.

5.3. Example 3

To demonstrate the applicability of the developed formulations for a somewhat more complicated problem that involves both the extra line integrals and the sub-regioning technique, the third example treated is a thin square plate partially loaded with an internal square volume heat source at its center as shown in Fig. 10. Also, all geometrical dimensions are shown in this figure. For thermal boundary conditions, two opposite sides EF and GH are prescribed with a temperature change $\Theta = 0°$ and

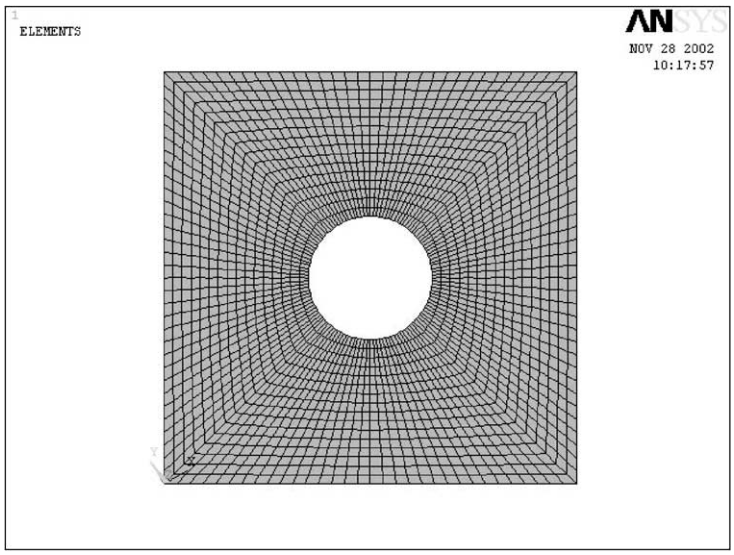

Fig. 5. FEM meshes by ANSYS to model the domain for Problem 2.

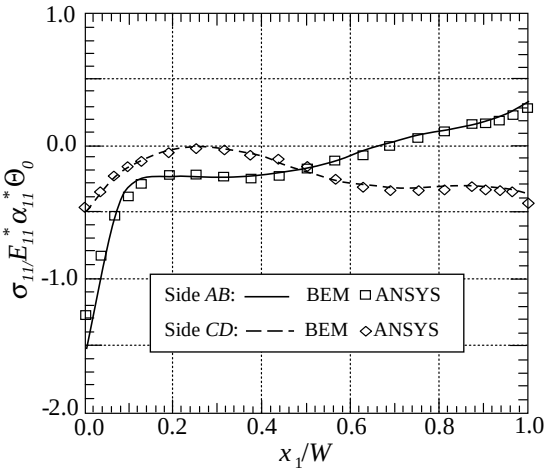

Fig. 6. Variations of normalized stresses, $\sigma_{11}/E^*_{11}\alpha^*_{11}\Theta_0$ ($\Theta_0 = 100°$), along AB and CD—Problem 2.

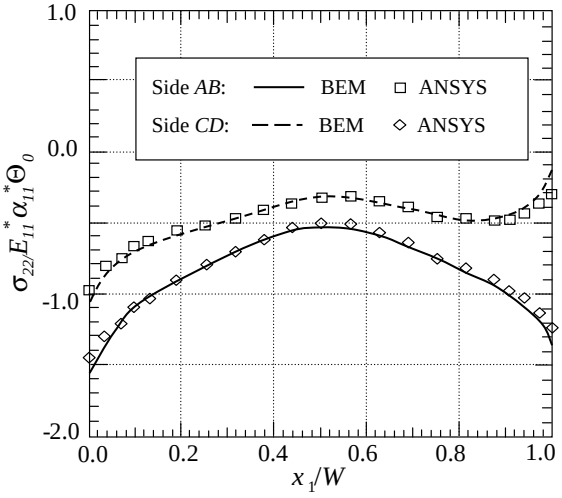

Fig. 7. Variations of normalized stresses, $\sigma_{22}/E^*_{11}\alpha^*_{11}\Theta_0$ ($\Theta_0 = 100°$), along sides AB and CD—Problem 2.

100°, respectively, while the other two surfaces are thermally insulated. For mechanical boundary conditions, the top and bottom surfaces are restrained from displacement in the x_2-direction like the preceding example, while the other two sides are free to move in any direction. Also, point E is restrained in the x_1-direction to prevent rigid body motion. To demonstrate the generality as well as the mathematical soundness of the proposed scheme for dealing with an arbitrary non-uniform volume heat source, the heat generation rate of the volume heat source is arbitrarily chosen to have a distribution described by

$$H(x_1, x_2)/K^*_{22} = (153.28571 - 32.21429x_1^2)\sin(x_2) + 153.90571x_1\cos(x_2) \tag{43}$$

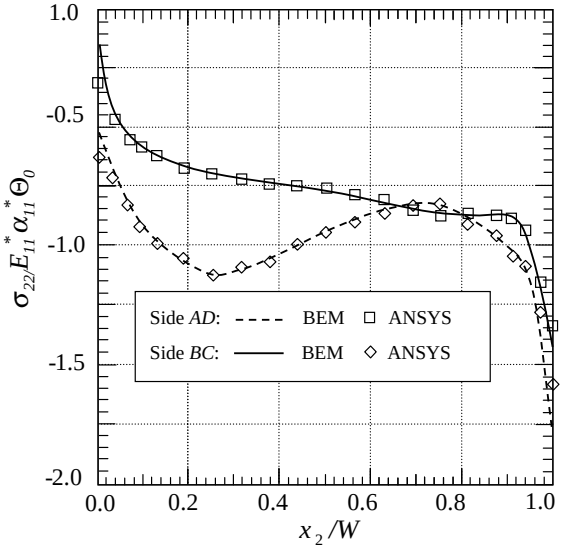

Fig. 8. Variations of normalized stresses, $\sigma_{22}/E_{11}^{*}\alpha_{11}^{*}T_0$ ($\Theta_0 = 100°$), along sides AD and BC—Problem 2.

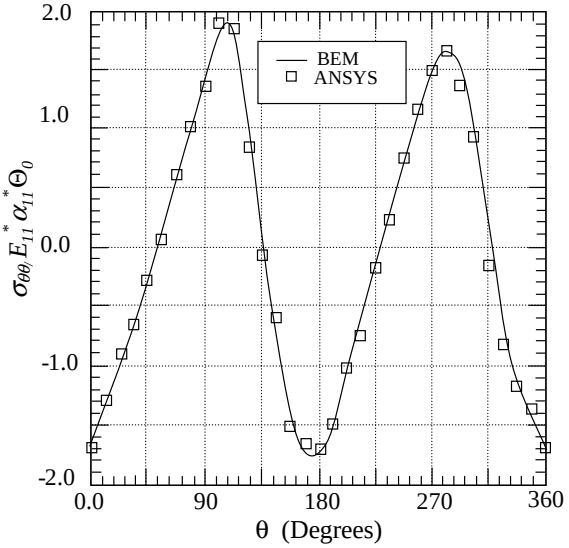

Fig. 9. Variations of normalized hoop stresses, $\sigma_{\theta\theta}/E_{11}^{*}\alpha_{11}^{*}\Theta_0$ ($\Theta_0 = 100°$), along the circumference of the hole for Problem 2.

where both x_1 and x_2 are bounded by $x_1, x_2 \in [0.7, 1.3]$. For visualization of the distribution of the heat generation rate, the distribution contours are also plotted in Fig. 10 with darker regions showing higher heat generation rates. By the conventional BEM sub-regioning technique to treat the region with and without a volume heat source as a separate sub-domain, a total of 72 quadratic isoparametric elements with 144 nodes are applied to model the boundaries of both sub-regions as shown in Fig. 11. In a similar manner

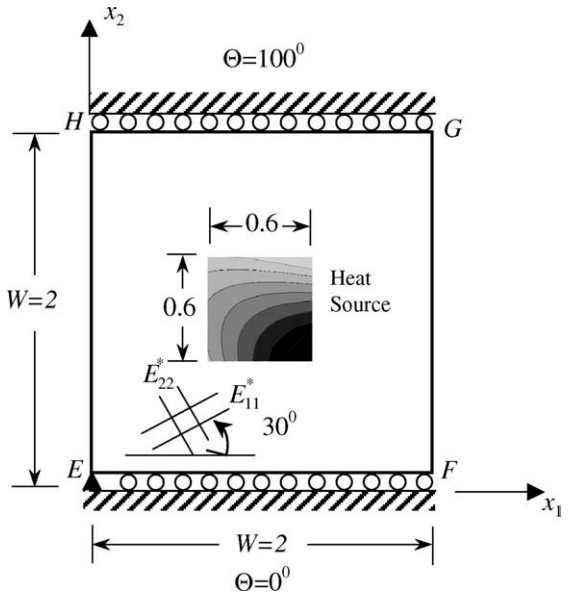

Fig. 10. A thin anisotropic plate subjected to an internal square volume heat source.

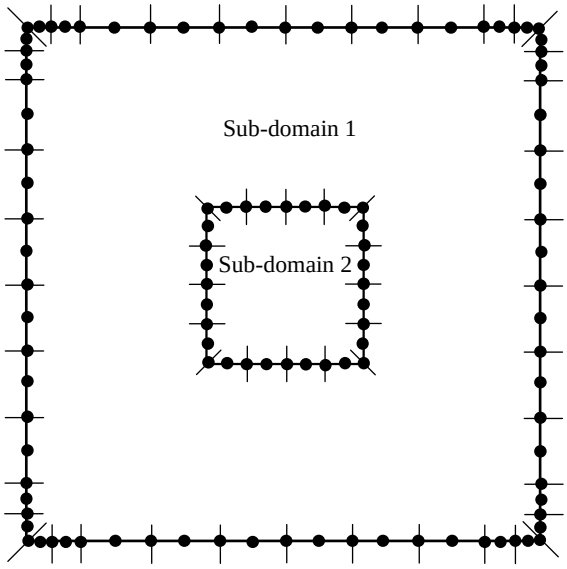

Fig. 11. Boundary element meshes to model the domain for Problem 3.

as the preceding example, the extra line integrals are involved to deal with the thermal loading for the outside domain, while the other sub-domain with an internal volume heat source is treated using the series of transformed boundary integrals ($n = 7$), yet without the involvement of the extra line integrals. Again, the problem is first solved for the associated temperature field and its spatial gradients at all nodes including

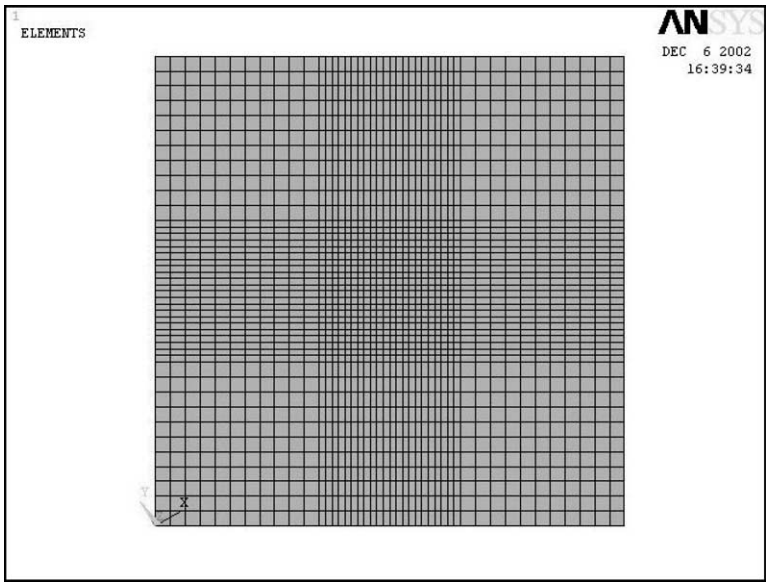

Fig. 12. FEM meshes by ANSYS to model the domain for Problem 3.

the boundary ones as well as those interior ones required by the extra line integrals. Then, by the BEM sub-regioning technique with the same mesh discretisation, the boundary integral equation, Eq. (39), is solved for the thermal stresses at all boundary nodes. As shown in Fig. 12, a total of 1936 PLANE77 elements are used in ANSYS to model the domain. The normalized stresses, $\sigma_{11}/E^*_{11}\alpha^*_{11}\Theta_0$ and $\sigma_{22}/E^*_{11}\alpha^*_{11}\Theta_0$, along EF and GH are calculated and plotted respectively in Figs. 13 and 14 for both results obtained by BEM and

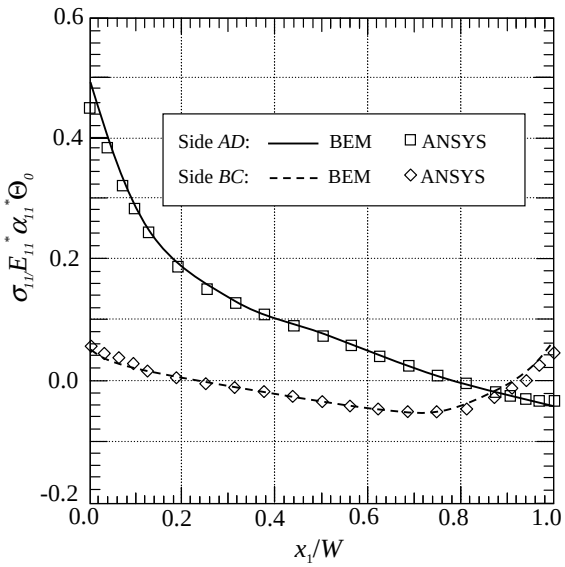

Fig. 13. Variations of normalized stresses, $\sigma_{11}/E^*_{11}\alpha^*_{11}\Theta_0$ ($\Theta_0 = 100°$), along EF and GH for Problem 3.

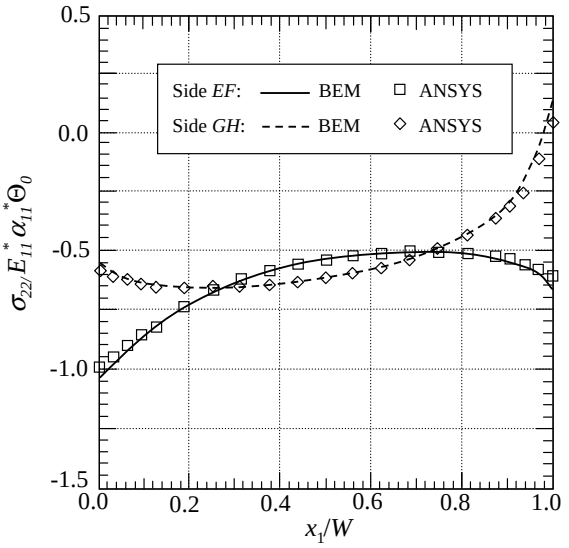

Fig. 14. Variations of normalized stresses, $\sigma_{22}/E_{11}^{*}\alpha_{11}^{*}\Theta_0$ ($\Theta_0 = 100°$), along sides EF and GH for Problem 3.

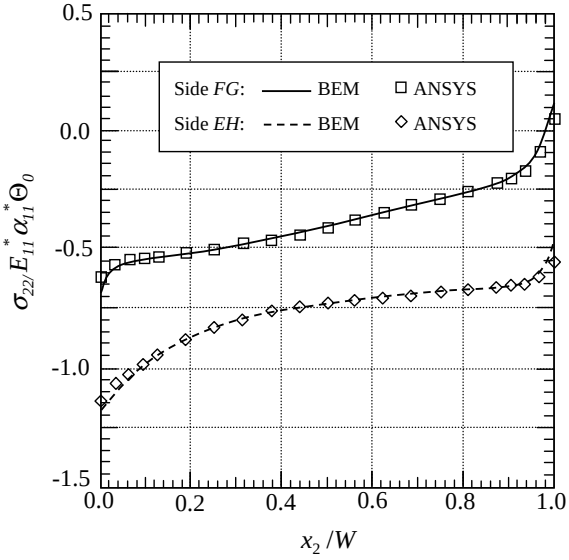

Fig. 15. Variations of normalized stresses, $\sigma_{22}/E_{11}^{*}\alpha_{11}^{*}\Theta_0$ ($\Theta_0 = 100°$), along sides FG and EH for Problem 3.

FEM; the variations of the normalized stresses, $\sigma_{22}/E_{11}^{*}\alpha_{11}^{*}\Theta_0$, along FG and EH are plotted in Fig. 15. Again, the excellent agreement between both results obtained by BEM and FEM shows the veracity of the developed formulations.

6. Conclusions

In the boundary element method for elastostatics, thermal effects are well known to manifest themselves as additional volume integrals in the direct formulations of the boundary integral equation. The success of applying the exact transformation method to treat the 2D thermoelasticity is not achieved until very recently. In this paper, the work to treat the problem of 2D anisotropic thermoelasticity is further extended by MRM to consider the effect of an internal non-uniform volume heat source with an arbitrary heat generation rate. By successively applying the exact transformation method to consider the effect of an internal arbitrary volume heat source, the volume integral arising from the thermal loading is transformed into an infinite series of boundary ones with higher-order fundamental functions given by recursive formulations. Due to the nature of fast convergence of the developed recursive formulations, the infinite series will, in general, converge rapidly with at most seven loops for an arbitrary continuous heat source function. Three numerical examples are given to demonstrate the veracity as well as the generality of the developed formulations.

Acknowledgement

Authors gratefully acknowledge the financial support by the National Science Council of Taiwan, Republic of China (grant number: NSC-91-2212-E-035-007).

References

Camp, C.V., Gipson, G.S., 1992. Boundary Element Analysis of Nonhomogeneous Biharmonic Phenomena. Springer-Verlag, Berlin.

Danson, D., 1983. Linear isotropic elasticity with body forces. In: Brebbia, C.A. (Ed.), Progress in Boundary Element Methods. Pentech Press, London.

Deb, A., Banerjee, P.K., 1990. BEM for general anisotropic 2D elasticity using particular integrals. Commun. Appl. Num. Mech. 6, 111–119.

Deb, A., Henry Jr., D.P., Wilson, E.B., 1991. Alternative BEM formulation for 2D and 3D thermoelasticity. Int. J. Solids Struct. 27, 1721–1738.

Dhaliwal, R., Sherief, H., 1980. Generalized thermoelasticity for anisotropic media. Quart. Appl. Math. 33, 1–8.

Gipson, G.S., Camp, C.V., 1985. Effective use of Monte Carlo quadrature for body force integrals occuring in integral form of elastostatics. In: Proceedings of the Seventh International Conference On Boundary Elements, pp. 17–26.

Lachat, J.C., 1975. Further development of the boundary integral technique for elastostatics, Ph.D. Thesis, Southampton University.

Nardini, D., Brebbia, C.A., 1982. A new approach to free vibration analysis using boundary elements. In: Boundary Element Methods in Engineering. Computational Mechanics Publications and Springer-Verlag, Southampton and Berlin.

Nowak, A.J., 1989. The multiple reciprocity method of solving transient heat conduction problems. In: Boundary Elements XI, vol. 2. Computational Mechanics Publications and Springer-Verlag, Southampton and Berlin.

Nowak, A.J., Brebbia, C.A., 1989. The multiple reciprocity method: A new approach for transforming BEM domain integrals to the boundary. Eng. Anal. 6 (3), 164–167.

Rizzo, F.L., Shippy, D.J., 1977. An advanced boundary integral equation method for three-dimensional thermoelasticity. Int. J. Numer. Methods Eng. 11, 1753–1768.

Sherief, H.H., Magahed, F.F., 1999. A two-dimensional thermoelasticity problem for a half space subjected to heat sources. Int. J. Solids Struct. 36 (9), 1369–1382.

Shiah, Y.C., Tan, C.L., 1999a. Exact boundary integral transformation of the thermoelastic domain integral in BEM for general 2D anisotropic elasticity. Computat. Mech. 23, 87–96.

Shiah, Y.C., Tan, C.L., 1999b. Determination of interior point stresses in two-dimensional BEM thermoelastic analysis of anisotropic bodies. Int. J. Solids Struct. 37, 809–829.

Shiah, Y.C., Tan, C.L., 1997. BEM treatment of two-dimensional anisotropic field problems by direct domain mapping. Eng. Anal. Boundary Elements 20, 347–351.

Tan, C.L., 1983. Boundary integral equation stress analysis of a rotating disc with corner crack. J. Strain Anal. 18, 231–237.

Tan, C.L., Gao, Y.L., Afagh, F.F., 1992. Anisotropic stress analysis of inclusion problems using the boundary integral equation method. J. Strain Anal. 27 (2), 67–76.

Zhang, J.J., Tan, C.L., Afagh, F.F., 1996a. An argument redefinition procedure in the BEM for 2D anisotropic elastostatics with body forces. In: Meguid, S.A. (Ed.), Proceedings of the Symposium on Mechanics in Design, Toronto, May 6–9, vol. 1, pp. 349–358.

Zhang, J.J., Tan, C.L., Afagh, F.F., 1996b. A general exact transformation of body-force volume integral in BEM for 2d anisotropic elasticity. Computat. Mech. 19, 1–10.

Zhang, J.J., Tan, C.L., Afagh, F.F., 1997. Treatment of body-force volume integrals in BEM by exact transformation for 2D anisotropic elasticity. Int. J. Numer. Methods Eng. 40, 89–109.